Journal of Molecular Graphics and Modelling 28 (2009) 270–277

Contents lists available at ScienceDirect

Journal of Molecular Graphics and Modelling

journal homepage: www.elsevier.com/locate/JMGM

Conformational flexibility decreased due to Y67F and F82H mutations in cytochrome *c*: Molecular dynamics simulation studies

Sarkkarai Raja Singh [a], Subash Prakash [a], Veerapandy Vasu [b], Chandran Karunakaran [c,*]

[a] *Biomedical Research Laboratory, Department of Physics, VHNSN College, Virudhunagar 626 001, India*
[b] *School of Physics, Madurai Kamaraj University, Madurai 625 021, India*
[c] *Biomedical Research Laboratory, Department of Chemistry, VHNSN College, Virudhunagar 626 001, India*

ARTICLE INFO

Article history:
Received 26 January 2009
Received in revised form 17 July 2009
Accepted 3 August 2009
Available online 8 August 2009

Keywords:
Cytochrome *c*
Molecular dynamics
Mutants
Essential dynamics
Conformational flexibility

ABSTRACT

Cytochrome *c* (cyt *c*), a mitochondrial protein, has dual functions in controlling both cellular energetic metabolism and apoptosis (programmed cell death). During apoptosis, cyt *c* (Fe^{3+}) released into the cytosol initiates caspase activation leading to apoptosis. Since, X-ray crystallography gives only the static structure, we report here the dynamic behavior of holo and apo wild type (WT), Y67F and F82H mutant cyt *c*'s (Fe^{3+}) in their apoptotic states. Four nanosecond MD simulations were run for holo WT, Y67F and F82H cyt *c*'s with and without Fe···S (Met-80) bond and also for apo WT and mutated cyt *c*'s (Y67F and F82H) in water using GROMOS96 force field. Mutations of Y67F and F82H resulted in the decrease of backbone and Cα RMSDs, and radii of gyration (backbone and protein) in both the holo and apo forms. MD and ED results revealed that the flexibility of mutated holo cyt *c*'s decreased perhaps affecting their ability to take part in mitochondrial electron/proton transfer process. Without Fe···S bond, the backbone and Cα RMSD increased in holo cyt *c*'s perhaps resulting in enhanced peroxidase activity. ED revealed that four to six eigenvectors involved in over all motions of holo cyt *c*'s without Fe···S bond, and six to eight eigenvectors in apo cyt *c*'s in comparison to three to four eigenvectors for holo cyt *c*'s with Fe···S bond.

1. Introduction

Cytochrome *c* (cyt *c*), mediates electron transfer from cyt *c* reductase to cyt *c* oxidase during aerobic respiration, and also apoptosis [1–4]. Cyt *c* consists of a single polypeptide chain containing 104 amino acid residues and a series of five α-helices and six β-turns [5]. Crystal structure of horse heart holo cyt *c* (pdb code 1hrc) revealed that the heme group, which is located in a groove and almost completely buried inside the protein, is nonplanar and somewhat distorted into shaddle-shape geometry [6]. The oxidized species (Fe^{3+}) are also more mobile than the reduced one, particularly in the millisecond time scale and on the time scale of $^1H/^2H$ exchange [7]. The net charge of heme in reduced state (Fe^{2+}) is neutral whereas that in oxidized state (Fe^{3+}) is +1e. X-ray crystallography provides an excellent method for the determination of high-resolution structures. It generates a static picture of a protein and, in general, provides little information on protein dynamics. Experimentally, a number of different nuclear magnetic resonance (NMR) techniques have been used to obtain information on the molecular motions within proteins on different time scales [8]. The number of proteins on which such studies can be performed, however, is limited. The use of computer simulations to probe protein internal motions, using existing structural information, is, therefore, proving extremely fruitful. However, in order to extract useful information about the dynamics observed during the course of these simulations, mathematical models must be employed [8].

Conformational flexibility perhaps plays an essential role in electron transfer process. Here, we have used the MD simulations to understand the various structural and dynamical properties of holo and apo forms of WT, Y67F and F82H cyt *c*'s. These mutant proteins have earlier been reported to be defective in their electron and proton transfer abilities and also causing apoptosis [9]. The Fe···S (Met-80) bond between the heme and the protein-based Met-80 ligand is thought to play a critical role in the redox properties of the cofactor [10,11]. Met-80 also plays an important role in folding, in which the final step requires this ligand to replace His-33 at the iron center, a rearrangement that has been suggested to be strongly coupled to backbone folding [12]. IR experiments have been used to study hemoprotein ligands such as CO and NO, but experiments to observe protein based ligands such as Met-80 in cyt *c* have not been possible. The details of how this critical

* Corresponding author. Present address: Biophysics Department, Medical College of Wisconsin, Milwaukee, WI 53226, United States. Tel.: +1 414 456 4034.
E-mail address: ckaru2000@gmail.com (C. Karunakaran).

1093-3263/$ – see front matter © 2009 Elsevier Inc. All rights reserved.
doi:10.1016/j.jmgm.2009.08.005

residue contributes to the biological functions or folding of this protein have remained obscure [13]. Therefore, we carried out here the MD simulations of holo WT, Y67F and F82H cyt *c*'s with and without Fe···S (Met-80) bond. The present MD and ED studies revealed that the conformational flexibility of mutated holo and apo cyt *c*'s considerably reduced compared to holo and apo WT cyt *c*'s and their implications in electron/proton transfer processes are discussed.

2. Methodology

2.1. Molecular dynamics

The starting structure for the first simulation was taken from the 1.94 Å resolution refined structure of holo protein horse heart cyt *c* [5]. The mutated proteins were constructed using the interactive computer graphics package Swiss pdb viewer v 3.6 [14] by replacing Tyr-67 residue in the holo WT crystal structure with Phe and by replacing Phe-82 residue with His. A covalent bond between Met-80 sulphur and the heme-105 iron was maintained in first case and is removed in second case. Nine simulations were performed, each of four nanoseconds for holo WT, Y67F and F82H cyt *c*'s [with and without Fe···S (Met-80) bond] and of apo forms of WT, Y67F and F82H cyt *c*'s using GROMOS96 force field in water solvent using the GROMACS 3.2.1 package of programs [15–18]. In this simulation work, we consider the Fe of heme is in oxidized state (Fe^{3+}). The scaled mulliken charges for the heme prosthetic group in oxidized state were obtained from the theoretical work done by Autenrieth et al. [19]. The proteins were simulated at pH 7.0. Each structure was fully solvated with SPC water [20] in a box with sides 3.668 nm × 3.049 nm × 3.651 nm with box angles 90° for each side. The number of solvent molecules in the MD simulations used was 3663 for holo form and 3676 for apo form cyt *c*'s.

A steepest descent algorithm was used for energy minimization. The maximum step size for energy minimization was 0.01 nm. The tolerance was 3000 kJ/mol/nm. The protein has a net charge of +8e. Only one protein molecule was considered in the simulations. Accurate simulation of protein dynamics requires the inclusion of the model of, at least, a neutralizing counter ions atmosphere. In our system, eight Cl^- ions were introduced by replacing eight solvent molecules with the highest electrostatic potential. After including these counter ions, protein had net charge zero. Position restrained MD was then performed before MD simulation. It involves restraining (partially freezing) the atom positions of the macromolecule while simultaneously allowing the solvent to move freely in the simulation. In all simulations, the temperature was maintained at 300 K by weak coupling to an external temperature bath [21] with a coupling constant 2 fs, equal to the time step. The protein and the rest of the system were coupled separately to the temperature bath. The SHAKE algorithm [22] was used to constrain all bonds. For the water molecules, the SETTLE algorithm [23] was used. A dielectric permittivity, $\varepsilon_r = 1$, and a time step 2 fs were used. During MD simulations, data were collected for every 500 ps. A twin range cut-off was used for the calculation of the non-bonded interactions. The short range cut-off radius was set to 0.9 nm and the long range cut-off radius to 1.4 nm for both Coulombic and Lennard-Jones interactions.

2.2. Essential dynamics

The ED method is based on the diagonalization of the covariance matrix, built from the atomic fluctuations in a MD trajectory from which overall translational and rotational motions have been removed [24]:

$$C_{ij} = \langle \frac{X_i - X_{i,0}}{X_j - X_{j,0}} \rangle \quad (1)$$

where X are the x-, y- and z-coordinates of the atoms fluctuating around their average positions (X_0) and $\langle \ldots \rangle$ denote an average over time. To construct the protein covariance matrices, we have used Cα atoms trajectory. Indeed it has been shown that the Cα atoms contain all the information for a reasonable description of the protein large concerted motion [25].

Covariant matrices were constructed and analyzed for both cases, using GROMACS 3.2.1 package [15–18]. Upon diagonalization of the covariance matrix, a set of eigenvalues and eigenvectors is obtained. The eigenvectors of the covariance matrix correspond to direction in a $3N$ dimensional space (where N is the number of Cα atoms), and motions along single eigenvector correspond to concerted fluctuations of atoms. Our system contained 104 Cα atoms, having 312 position coordinates. The eigenvalues represent the total mean square fluctuation of the system along the corresponding eigenvectors. If the eigenvectors are ordered according to decreasing eigenvalues, the first one describes the largest scale correlated motions, whereas the last one will correspond to small-amplitude vibrations. By projecting all frames from the MD trajectory on an eigenvector, a new trajectory can be generated which, upon visual inspection, reveals the correlated modes, e.g. the modes in which one part of a cyt *c* protein tends to act concertedly with another [25].

3. Results and discussion

MD simulations were performed and analyzed to understand the protein internal motions and conformational changes within nanosecond time scale for holo WT, Y67F and F82H cyt *c*'s with Fe···S (Met-80) bond. Structural properties of the three holo cyt *c*'s with Fe···S (Met-80) bond are presented in Fig. 1. The summary of data obtained for the three holo cyt *c*'s are presented in Tables 1–3.

3.1. MD simulations of Y67F and F82H with Fe···S (Met-80) bond

To check the stability of the simulations, the root mean square deviations (RMSDs) of the backbone and Cα atoms with respect to the starting X-ray structure, radii of gyration R_g (protein and backbone) and Solvent Accessible Surface Area ($SASA_{total}$) of protein [26,27] were calculated and monitored for holo WT, Y67F and F82H cyt *c*'s, over the course of simulations and are presented in Table 1.

The RMSDs of the backbone atoms and Cα atoms with respect to the starting structure for the three simulations as a function of time are plotted in Fig. 1a and b. The equilibration time (backbone atoms) for holo WT cyt *c* is 500 ps whereas for holo Y67F and F82H cyt *c*'s these values are 250 ps and 100 ps respectively. After 500 ps, the RMSD values for holo WT cyt *c* undergo larger fluctuations with respect to the first portion of the simulations. The relatively high values and the irregular profile of the plots reflect the structural changes of highly flexible protein regions. The average value of RMSD for backbone atoms in holo WT cyt *c* is 0.0670 nm. Whereas the average values of RMSD for backbone atoms in holo Y67F and F82H cyt *c*'s are 0.0546 nm and 0.0443 nm respectively. The plot of radius of gyration R_g (protein) versus time is presented in Fig. 1c. It is evident that the R_g value of protein for holo WT cyt *c* varies between 1.2861 nm and 1.2996 nm, for holo Y67F cyt *c* this value varies between 1.2842 nm and 1.2937 nm while for holo F82H cyt *c* this variation is between 1.2821 nm and 1.2937 nm. The average values of radius of gyration (R_g-protein) for holo WT cyt *c* and mutated holo cyt *c*'s are 1.2949 nm, 1.2886 nm and 1.2875 nm

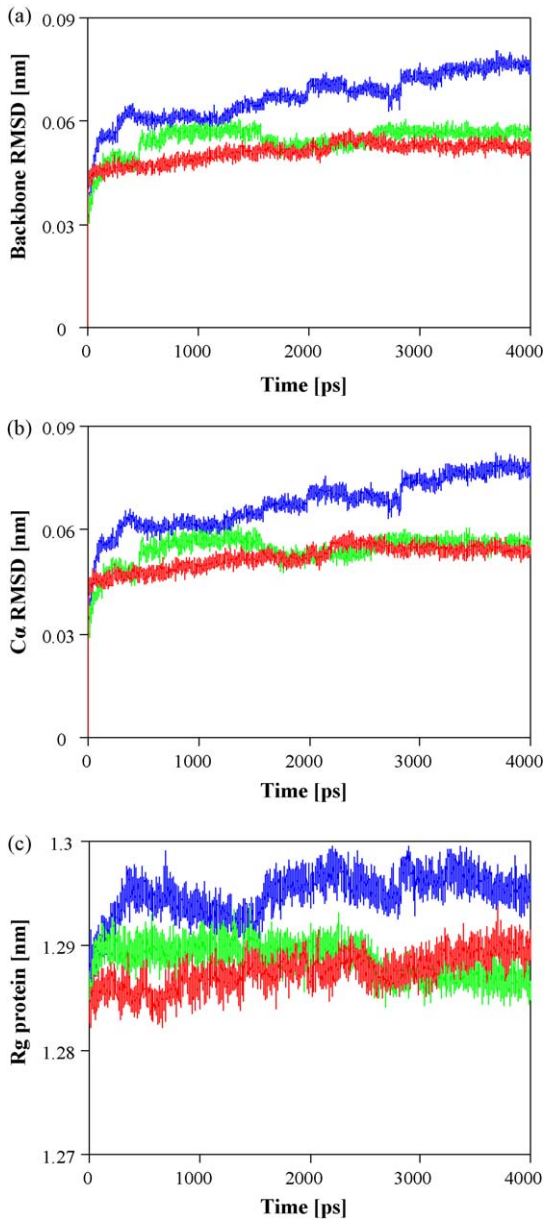

Fig. 1. Evolution of structural properties over time: (a) backbone RMSD, (b) Cα RMSD, (c) radius of gyration R_g (protein); blue: WT, bright green: Y67F, and red: F82H holo cyt *c*'s [with Fe···S (Met-80) bond].

respectively. These data revealed that the stability of holo cyt *c*'s increased upon mutation. From the crystal structure, the R_g (protein) value for holo WT cyt *c* is 1.26 nm [28].

Interesting information comes from the root mean square fluctuations (RMSFs) of each amino acid, shown in Fig. 2 for the holo WT, Y67F and F82H cyt *c*'s. The RMSF differences indicate that the dynamics of the core were different for holo WT, Y67F and F82H cyt *c*'s. For holo WT cyt *c*, there are four loop regions that display larger flexibility. These four regions comprise residues 21–35 (loop-1), 36–59 (loop-2), 70–85 (loop-3) and 87–102 (C-terminal helix). For holo Y67F and F82H cyt *c*'s, the flexibility is decreased. The increasing deviations observed along the trajectory for holo WT cyt *c* are related to deformations of the loop-1, loop-2, loop-3 and C-terminal helix regions. The three models exhibited different dynamical behavior. These data further revealed that the flexibility of holo WT cyt *c* is larger than mutated holo cyt *c*'s. The increase in flexibility and the resulting decrease in stability of the Fe^{3+} holo WT cyt *c* is a well documented property of *eukaryotic* cyt *c* [29–31].

Table 1
Time averaged structural properties calculated for WT, Y67F and F82H holo cyt *c*'s [with Fe···S (Met-80) bond].

Properties	WT cyt *c*	Y67F cyt *c*	F82H cyt *c*
Backbone RMSD (nm)	0.0670 (0.01)	0.0546 (0.01)	0.0509 (0.01)
Cα-RMSD (nm)	0.0676 (0.01)	0.0542 (0.01)	0.0520 (0.01)
R_g-protein (nm)	1.2949 (0.01)	1.2886 (0.01)	1.2875 (0.01)
R_g-backbone (nm)	1.2573 (0.01)	1.2464 (0.01)	1.2481 (0.01)
$SASA_{total}$ (nm^2)-protein	67.80 (0.66)	67.14 (0.60)	66.83 (0.65)

Standard deviations are given in parentheses.

Table 2
Distance variation of active site environment [with Fe···S (Met-80) bond].

Distance between the residues	WT cyt *c* (nm)	Y67F cyt *c* (nm)	F82H cyt *c* (nm)
Res67 and Cys-14	1.1993 (0.03)	1.2232 (0.02)	1.1605 (0.03)
Res67 and Cys-17	1.3756 (0.03)	1.4063 (0.02)	1.3790 (0.02)
Res67 and His-18	1.3012 (0.02)	1.2823 (0.02)	1.2458 (0.02)
Res67 and Met-80	0.6938 (0.01)	0.7290 (0.01)	0.7372 (0.01)
Res67 and Res82	0.9073 (0.02)	0.9316 (0.02)	0.9309 (0.02)
Met-80 and Res82	0.6157 (0.02)	0.6166 (0.01)	0.5749 (0.02)
Cys-14 and heme	0.7952 (0.01)	0.7959 (0.01)	0.7761 (0.01)
Cys-17 and heme	0.7048 (0.01)	0.7015 (0.03)	0.6771 (0.01)
His-18 and heme	0.6664 (0.01)	0.6539 (0.02)	0.6046 (0.01)
Res67 and heme	0.7416 (0.01)	0.7738 (0.01)	0.7627 (0.01)
Met-80 and heme	0.4175 (0.01)	0.4246 (0.01)	0.4377 (0.02)
Res82 and heme	0.7966 (0.01)	0.7993 (0.01)	0.7897 (0.01)

Within parentheses standard deviation values. For WT and F82H holo cyt *c*'s Res67–Tyr and Y67F holo cyt *c* Res67–Phe. For WT and Y67F holo cyt *c*'s Res 82–Phe and F82H holo cyt *c* Res 82–His.

Table 3
Average distance between the two pairs of the residues in holo cyt *c*'s Trp-59 (**A**) and Tyr-74 (**B**) is denoted as *X* and the residues Tyr-67 (**C**) and Met-80 (**D**) denoted as *Y* [with Fe···S (Met-80) bond].

Cyt *c*	Average distance between **AB** (*X*) in nm	Average distance between **CD** (*Y*) in nm	Correlation coefficient
WT	0.8641 (0.03)	0.6938 (0.01)	−0.2574
Y67F	0.8831 (0.02)	0.7291 (0.01)	0.1428
F82H	0.9070 (0.01)	0.7372 (0.02)	−0.0849

The standard deviation values are given in parentheses.

Distance variations in active site environment are presented in Table 2. From Table 2, the distances of the active site residues Cys-14, Cys-17, Met-80, Phe-82 and Heme-105 with Phe-67 increased in holo Y67F cyt *c*. Also, the distances of the residues Met-80, Phe-82 and Heme-105 with Tyr-67 increased in holo F82H cyt *c*. This revealed that the holo Y67F and F82H cyt *c*'s may be in open active

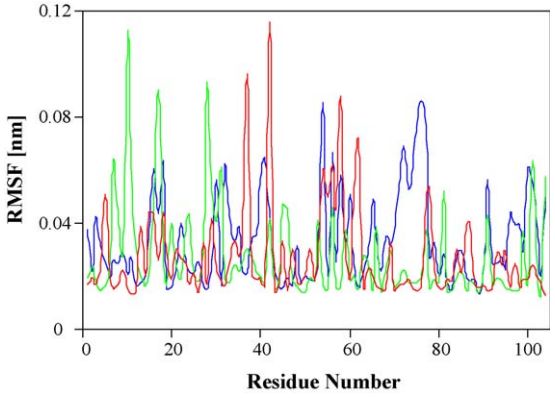

Fig. 2. RMSF of backbone atoms as a function of amino acids; blue: WT, bright green: Y67F, and red: F82H holo cyt *c*'s [with Fe···S (Met-80) bond].

site conformation upon mutation, and leading to enhanced peroxidase activity reported earlier [32]. In holo WT cyt *c*, the heme group is covalently linked with Cys-14 and Cys-17. The axial ligands of the heme iron are His-18 and Met-80. The distance between His-18 and Heme-105 decreased largely in holo F82H cyt *c*. There is no change in distance between Phe-82 and Heme-105 in holo WT and Y67F cyt *c*'s, whereas the distance between His-82 and Heme-105 decreased in holo F82H cyt *c* which revealed that, the axial ligands of the heme iron are His-18 and His-82 in holo F82H cyt *c*. These results are agreed with the experimental work done by Zheng et al. [33].

3.2. Distance analysis between the critical residues with Fe···S (Met-80) bond

Electrons from mitochondrial cyt *c* reductase are transmitted to ferricytochrome *c* by different pathway than electrons from ferrocytochrome *c* to cyt *c* oxidase. According to Takano et al. [34], starting with the ferric protein, the electron transferred from the cyt *c* reductase to Tyr-74 of holo WT cyt *c* is next moved to the parallel ring system of Trp-59, a second electron is then transferred from Tyr-67 to the heme, possibly by way of the sulphur of Met-80. The conformation changes from state ferric to the ferrous state, which brings the aromatic rings of Trp-59 and Tyr-67 into parallel, enabling an electron to be transferred from the electron-rich Trp-59 to the electron-deficient Tyr-67, restoring electroneutrality [35].

So, we have measured the distances between the two pairs (**AB** and **CD**) of residues at every 1 ps time interval to check whether the distances are correlated or not, in three holo cyt *c*'s. The first pair is **A**, Trp-59 and **B**, Tyr-74. The second pair is **C**, Tyr-67, and **D**, Met-80. These four residues are directly involved in electron transfer from cyt *c* reductase to holo cyt *c*. The distance between the residues **A** and **B** is denoted as '*X*' and the distance between **C** and **D** as '*Y*'. The average values of *X* and *Y* for all the conformations along with their correlation coefficients are tabulated in Table 3. In holo WT cyt *c*, the '*X*' and '*Y*' values are significantly different and lower than that in holo Y67F and F82H cyt *c*'s. The distances *X* and *Y* increased in mutated holo cyt *c*'s, perhaps resulting in its inability to electron carrier as reported earlier [34,35].

3.3. Essential dynamics analysis with Fe···S (Met-80) bond

ED is a technique that allows the identification of the correlated motions of a protein during a trajectory generated by the simulation. After the removal of rotational motions, a covariance matrix was constructed for holo WT, Y67F and F82H cyt *c*'s using Eq. (1). The diagonalization of the matrix gave a set of eigenvectors/eigenvalues. Each eigenvector represents one single direction in multidimensional space whereas the eigenvalue is the amplitude of the motion along the eigenvector. The Cα displacement along each eigenvector can provide insights into the concerted motions of the protein.

The MD trajectories of holo WT, Y67F and F82H cyt *c*'s have been analyzed according to the ED approach. Eigenvalues for three holo cyt *c*'s calculated using Eq. (1), against the corresponding eigenvector index for the first ten modes of motion at different trajectory lengths are plotted in Fig. 3. There are only few eigenvectors with large eigenvalues, showing that the protein motion occurred mainly along very few directions in the essential subspace.

Total positional fluctuations as a function of increasing number of eigenvectors at different trajectory lengths are shown in Fig. 4 for three holo cyt *c*'s. It revealed that only three to four eigenvectors were needed to describe the essential motions in three holo cyt *c*'s, as shown in Fig. 4. Indeed, approximately 98% of the total motion is described by the first two to three eigenvectors

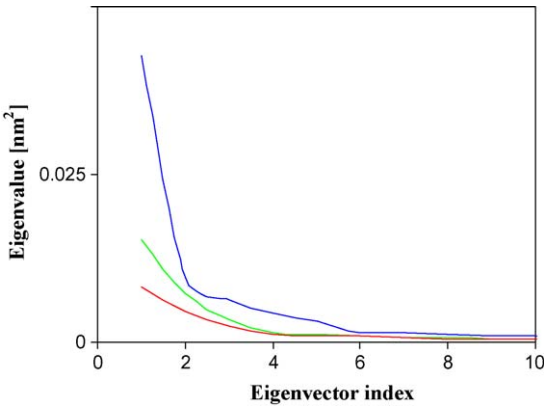

Fig. 3. Plot of eigenvalues corresponding to eigenvector index for the first ten modes of motion; blue: WT, bright green: Y67F, and red: F82H holo cyt *c*'s [with Fe···S (Met-80) bond].

for the three holo cyt *c*'s. Thus most of the internal motions of holo WT, Y67F and F82H cyt *c*'s represented by a subspace whose dimension is much smaller than original 3*N* configurational space.

Fig. 5 shows the Cα displacements along the four main eigenvectors. The essential motions identified are different for all three holo cyt *c*'s. The most flexible regions for holo WT cyt *c* comprises residues 37–45 (loop-2), 70–75 (70s helix) and 87–102 (C-terminal helix) for all of the first three eigenvectors. Fig. 5 clearly indicates that these regions are exploring a wide conformational space since their motions have large amplitude along all of the first three most important directions of the essential space. For holo Y67F cyt *c*, the N-terminal helix and loop-1 undergo largest movements while loop-2 and loop-3 undergo lesser movements. In holo F82H cyt *c* there is no concerted motion in N-terminal helix but there are lesser movements in C-terminal helix, loop-1, loop-2 and loop-3 regions. These data revealed that the concerted motions decreased considerably in mutated holo cyt *c*'s and in agreement with the MD analysis.

3.4. MD simulations of Y67F and F82H without Fe···S (Met-80) bond

In the native state of holo WT cyt *c*, the heme group in the protein is covalently attached to the His-18 and Met-80 residues. A number of kinetic studies suggest that under denaturing/apoptotic conditions the linkage of the heme group to Met-80 dissociated and was replaced by linkage to one of the other nearby available His residues [36,37].

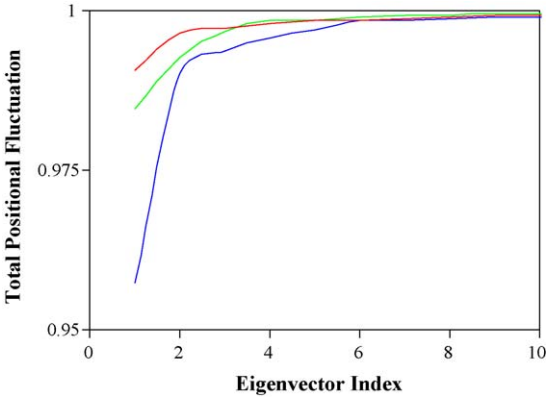

Fig. 4. Total positional fluctuations as a function of eigenvectors computed from Cα covariance matrices constructed from simulations of different trajectory lengths; blue: WT, bright green: Y67F, and red: F82H holo cyt *c*'s [with Fe···S (Met-80) bond].

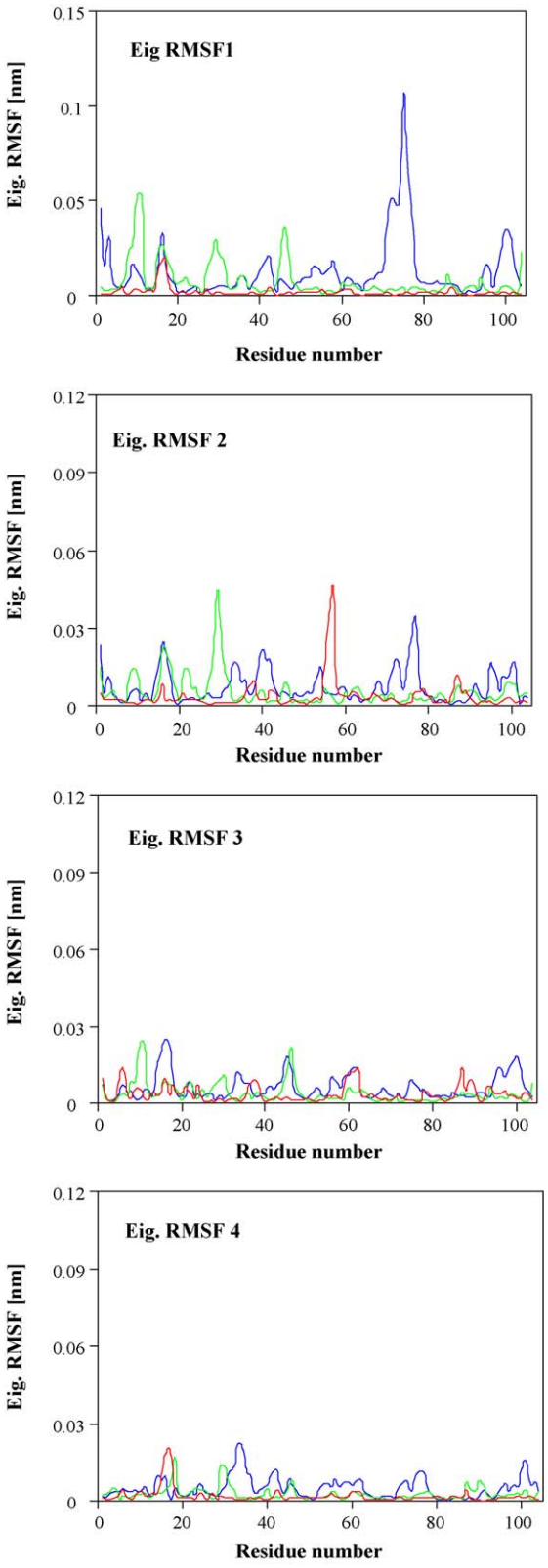

Fig. 5. RMSF per atom of eigenvectors as a function of Cα atoms; blue: WT, bright green: Y67F, and red: F82H holo cyt *c*'s [with Fe···S (Met-80) bond].

So, MD simulations of holo WT, Y67F and F82H cyt *c*'s were also performed without Fe···S (Met-80) bond. The RMSDs of the backbone and Cα atoms with respect to the starting structure, R_g (protein and backbone) and $SASA_{total}$ (protein) were also calculated and monitored for holo WT, Y67F and F82H cyt *c*'s, without Fe···S

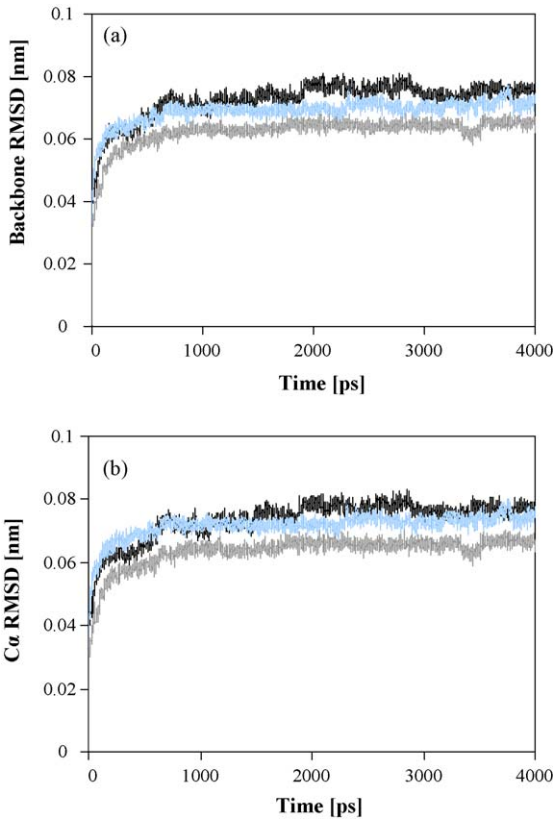

Fig. 6. Evolution of structural properties over time: (a) backbone RMSD and (b) Cα RMSD; black: WT, sky blue: Y67F, and grey: F82H holo cyt *c*'s [without Fe···S (Met-80) bond].

(Met-80) bond over the course of simulations and presented in Table 1S (See Supplementary Data). The average values of RMSD for the backbone atoms in holo WT, Y67F and F82H cyt *c*'s are 0.0724 nm, 0.0688 nm and 0.0624 nm respectively. These data revealed that the flexibility increased in three holo cyt *c*'s when the Fe···S (Met-80) bond is removed.

The RMSDs of the backbone atoms and Cα atoms with respect to the starting structure as a function of time for the three holo cyt *c*'s are presented in Fig. 6a and b. From Fig. 6a and b, the equilibration time (backbone and Cα atoms) for holo WT cyt *c* is 600 ps whereas for both holo Y67F and F82H cyt *c*'s these values are 300 ps respectively. These times are larger for three holo cyt *c*'s compared to the results of the MD simulation with Fe···S (Met-80) bond. The RMSFs of each amino acid are presented in Fig. 7 for

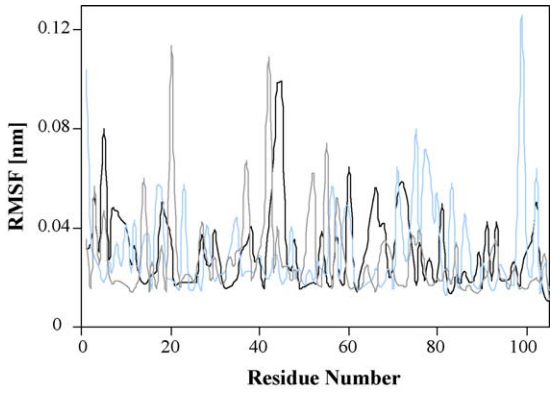

Fig. 7. RMSF of backbone atoms as a function of amino acids; black: WT, sky blue: Y67F, and grey: F82H holo cyt *c*'s [without Fe···S (Met-80) bond].

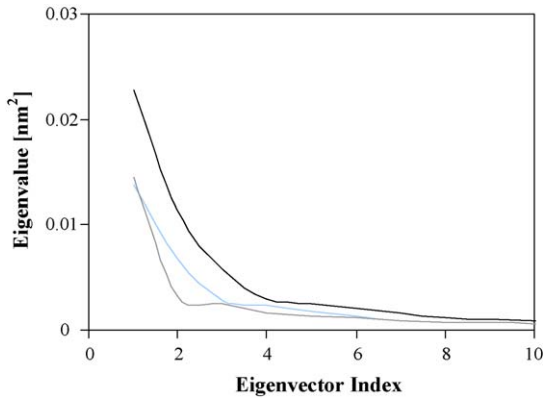

Fig. 8. Plot of eigenvalues corresponding to eigenvector index for the first ten modes of motion; black: WT, sky blue: Y67F, and grey: F82H holo cyt *c*'s [without Fe···S (Met-80) bond].

three holo cyt *c*'s without Fe···S (Met-80) bond. From Figs. 6a and 7, for holo WT, Y67F and F82H cyt *c*'s the RMSDs and the RMSFs increased, when there is no Fe···S (Met-80) bond.

The average values of *X* and *Y* for all the conformations along with their correlation coefficients are calculated and presented in Table 2S (See Supplementary Data). In holo WT cyt *c* (without Fe···S bond) the distance between Trp-59 and Tyr-74 (*X*) increased and the distance between Tyr-67 and Met-80 (*Y*) decreased. This revealed that Tyr-67 and Met-80 come closer to each other in the absence of Fe···S bond. In holo Y67F cyt *c* (without Fe···S bond) the distances *X* and *Y* increased, while in holo F82H cyt *c* (without Fe···S bond) these distances decreased. These data indicate that the electron transfer pathways may be affected [34,35].

The eigenvalues corresponding to eigenvector indices for the first ten modes of motion are plotted in Fig. 8 for three holo cyt *c*'s. Also, total positional fluctuations as a function of eigenvector indices are presented in Fig. 9. Figs. 8 and 9 revealed that four to six eigenvectors involved in concerted motion of the cyt *c*'s compared to three to four eigenvectors in holo cyt *c*'s in the presence of Fe···S (Met-80) bond.

The variations of RMSF per atom of eigenvectors as a function of Cα atoms for the first four eigenvectors are presented in Fig. 10. From Fig. 10, the RMSF per atom of eigenvectors is larger in three holo cyt *c*'s when there is no Fe···S (Met-80) bond. These fluctuations are larger due to the absence of Fe···S (Met-80) bond. Thus the removal of Fe···S (Met-80) bond perhaps led to increase in peroxidase activity.

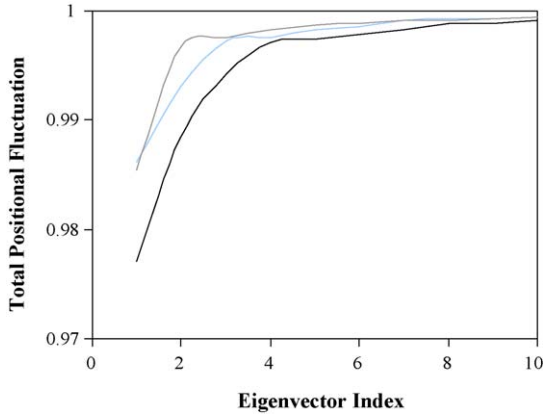

Fig. 9. Total positional fluctuations as a function of eigenvectors; black: WT, sky blue: Y67F, and grey: F82H holo cyt *c*'s [without Fe···S (Met-80) bond].

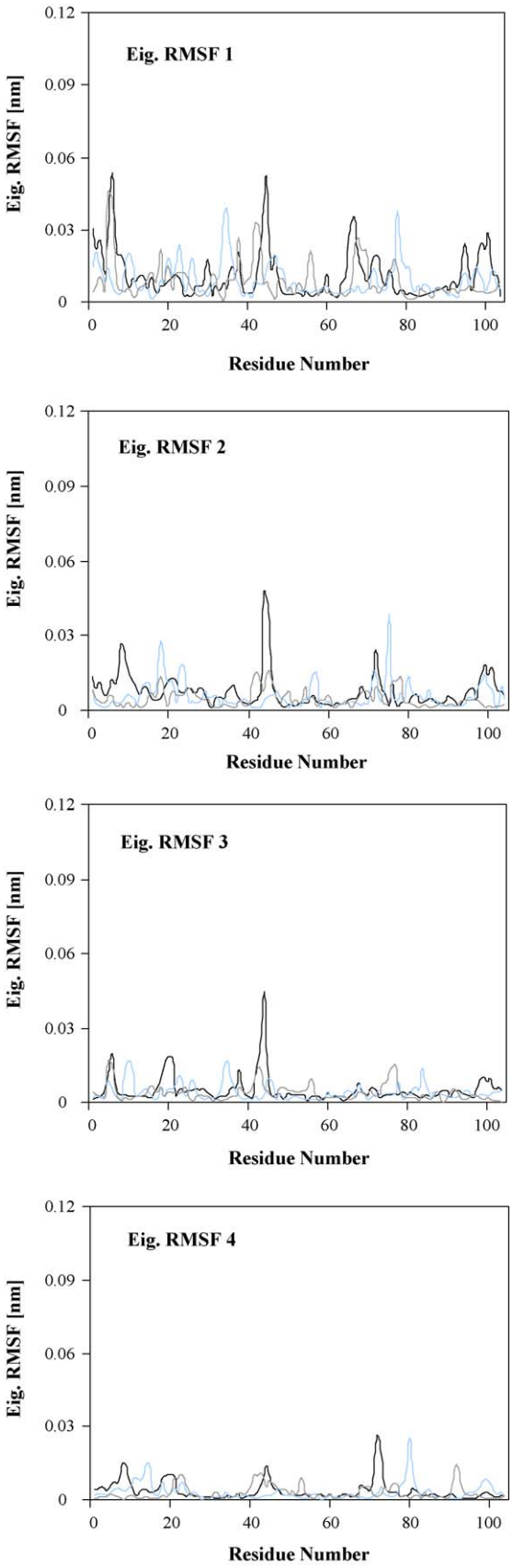

Fig. 10. RMSF per atom of eigenvectors as a function of Cα atoms; black: WT, sky blue: Y67F, and grey: F82H holo cyt *c*'s [without Fe···S (Met-80) bond].

3.5. MD simulations of apo forms of WT, Y67F and F82H cyt c's

Apocytochrome *c* is the precursor of the mitochondrial protein cytochrome *c*. Hence, MD simulations of apo (heme free) WT, Y67F and F82H cyt *c*'s were run and the results were analyzed. The RMSDs of the backbone and Cα atoms, R_g (protein and backbone) and $SASA_{total}$ (protein) were also calculated and monitored for apo WT, Y67F and F82H cyt *c*'s over the course of simulations as presented in Table 3S (See Supplementary Data). The RMS deviations of the backbone atoms with respect to the starting structure as a function of time for the three apo cyt *c*'s are presented in Fig. 1S (See Supplementary Data). The overall backbone RMS deviations reached equilibrated region after 350 ps, 300 ps and 300 ps respectively for apo WT, Y67F and F82H cyt *c*'s. The average values of backbone RMSD for apo WT, Y67F and F82H cyt *c*'s are 0.0551 nm, 0.0507 nm and 0.0622 nm respectively. This result revealed that the flexibility of apo WT and F82H cyt *c*'s is larger than apo Y67F cyt *c*. The root mean square fluctuations (RMSFs) of each amino acid are reported in Fig. 2S (See Supplementary Data). From Fig. 2S, the flexibility of apo WT cyt *c* is larger compared to apo Y67F and F82H cyt *c*'s. For apo WT cyt *c*, α-helices (N-terminal, C-terminal, 50s and 70s helices) show larger flexibility similar to holo WT cyt *c* compared to other regions. In apo Y67F and F82H cyt *c*'s loop-3 undergoes larger fluctuation and very small fluctuation in α-helices.

Conformational flexibility of three apo cyt *c*'s is checked by essential dynamics technique. The eigenvalues and total positional fluctuations as a function of eigenvector indices for the first twenty modes are plotted in Figs. 3S and 4S respectively (See Supplementary Data). This revealed that six to eight eigenvectors are involved in over all motions of apo cyt *c*'s compared to three to four eigenvectors in holo cyt *c*'s. Fig. 5S (See Supplementary Data) displays the displacement of Cα atoms, for the first six eigenvectors. The RMSF per Cα atom of apo WT cyt *c* is larger, compare to mutated apo cyt *c*'s.

4. Conclusions

In summary, the present MD simulations revealed that the conformational flexibility decreased and stability increased significantly in holo Y67F and F82H cyt *c*'s compared to holo WT cyt *c* in the presence of Fe···S (Met-80) bond. For holo WT cyt *c*, increasing mobility is due to the larger movements of loop-1, loop-2, loop-3 and C-terminal helix. Mutation caused especially open conformation at the heme active site perhaps resulting in reported enhanced peroxidase activity. In mutated holo cyt *c*'s, the distances between critical electron-transfer residues increased perhaps led to its inability to act as electron carrier causing its inactivation. ED revealed that the total positional fluctuations and RMSF per atom are mostly due to three to four eigenvectors when there is Fe···S (Met-80) bond, four to six eigenvectors in the absence of Fe···S (Met-80) bond and six to eight eigenvectors for apo cyt *c*'s. These studies suggest that the conformational flexibility may have implications in mitochondrial electron/proton transfer and peroxidase properties.

Appendix A. Supplementary data

Supplementary data associated with this article can be found, in the online version, at doi:10.1016/j.jmgm.2009.08.005.

References

[1] X. Hu, T. Ritz, A. Damjanovic, F. Autenrieth, K. Schulten, Photosynthetic apparatus of purple bacteria, Quart. Rev. Biophys. 35 (2002) 1–62.
[2] J. Berg, J. Tymoczko, L. Stryer, Biochemistry, W.H. Freeman and Company, New York, 2002.
[3] H.B. Gray, Biological inorganic chemistry at the beginning of the 21st century, Proc. Natl. Acad. Sci. U.S.A. 100 (2003) 3563–3568.
[4] Y.A. Shi, Structural view of mitochondria-mediated apoptosis, Nat. Struct. Biol. 8 (2001) 394–401.
[5] G.W. Bushnell, G.V. Louie, G.D. Brayer, High-resolution three dimensional Structure of horse heart Cytochrome *c*, J. Mol. Biol. 214 (1990) 585–595.
[6] L. Bu, J.E. Straub, Vibrational frequency shifts and relaxation rates for a selected vibrational mode in cytochrome *c*, Biophys. J. 85 (2003) 1429–1439.
[7] T.A. Lyons, G. Ratnaswamy, T.C. Pochapsky, Redox-dependent dynamics of putidaredoxin characterized by amide proton exchange, Protein Sci. 5 (1996) 627–639.
[8] N.J. Marianayagam, S.E. Jackson, Native-state dynamics of the ubiquitin family: implications for function and evolution, J. Roy. Soc. Interface 2 (2005) 47–54.
[9] E. Margoliash, S.F. Miller, J. Tullose, C.H. Kang, B.A. Feinberg, D.L. Brautigan, M. Morrison, Separate intramolecular pathways for reduction and oxidation of cytochrome *c* in electron transport chain reactions, Proc. Natl. Acad. Sci. U.S.A. 70 (11) (1973) 3245–3249.
[10] A.L. Raphael, H.B. Gray, Semisynthesis of axial-ligand (position 80) mutants of cytochrome *c*, J. Am. Chem. Soc. 113 (1991) 1038–1040.
[11] A.L. Raphael, H.B. Gray, Axial ligand replacement in horse heart cytochrome *c* by semisynthesis, Proteins Struct. Funct. Genet. 6 (1989) 338–340.
[12] W. Colón, L.P. Wakem, F. Sherman, H. Roder, Identification of the predominant non-native histidine ligand in unfolded cytochrome *c*, Biochemistry 36 (1997) 12535–12541.
[13] J.K. Chin, R. Jimenez, F.E. Romesberg, Direct observation of protein vibrations by selective incorporation of spectroscopically observable carbon–deuterium bonds in cytochrome *c*, J. Am. Chem. Soc. 123 (2001) 2426–2427.
[14] N. Guex, A. Diemand, T. Schwede, M.C. Peitsch, Swiss-Pdb Viewer: V 3.6, 2000.
[15] H.J.C. Berendsen, D. van der Spoel, R. van Drunen, GROMACS: a message-passing parallel molecular dynamics implementation, Comp. Phys. Commun. 91 (1995) 45–56.
[16] E. Lindahl, B. Hess, D. van der Spoel, GROMACS 3.0 a package for molecular simulation and trajectory analysis, J. Mol. Model. 7 (2001) 306–317.
[17] D. Van der Spoel, E. Lindahl, B. Hess, A.R. Van Buuren, E. Apol, P.J. Meulenhoff, D.P. Tieleman, A.L.T.M. Sijbers, A.K. Feenstra, R. Van Druunen, H.J.C. Berendsen, Groningnen Machine for Molecular Simulations, BIOSON Research Institute, Groningnen, the Netherlands, 2004.
[18] W.F. Van Gunstren, S.R. Billeter, A.A. Eising, P.H. Humberger, P. Kruger, A.E. Mark, W.R.P. Scott, I.G. Tironi, Biomolecular Simulation: The GROMOS96 Manual and User Guide, Hochschulverlag AG an der ETH, 1996.
[19] F. Autenrieth, E. Tajkhorshid, J. Baudry, Z. Luthey-Schulten, Classical force field parameters for the heme prosthetic group of cytochrome *c*, J. Comp. Chem. 25 (2004) 1613–1622.
[20] H.J.C. Berendsen, J.D.M. Postman, W.F. van Gunsteren, J. Hermans, Intermolecular forces. Interaction models for water in relation to protein hydration, Dordrecht: D. Reidel (1981) 331–342.
[21] H.J.C. Berendsen, J.D.M. Postman, W.F. van Gunsteren, A. Di Nola, J.R. Haak, Molecular dynamics with coupling to an external bath, J. Chem. Phys. 81 (1984) 3684–3690.
[22] J.P. Ryckaert, G. Ciccotti, H.J.C. Berendsen, Numerical integration of the Cartesian equations of motions of systems with constraints: molecular dynamics of n-alkanes, J. Comp. Phys. 23 (1977) 327–341.
[23] S. Miyamoto, P.A. Kollman, SETTLE: an analytical version of the SHAKE and RATTLE algorithms for rigid water molecules, J. Comp. Chem. 13 (1992) 952–962.
[24] C. Arcangeli, A. Rita Bizzarri, S. Cannistraro, Concerted motions in copper plastocyanin and azurin: an essential dynamics study, Biophys. Chem. 90 (2001) 45–56.
[25] A. Amadei, A.B.M. Linssen, H.J.C. Berendsen, Essential dynamics of proteins, Proteins Struct. Funct. Genet. 17 (1993) 412–425.
[26] F. Eisenhaber, P. Lijnzaad, P. Argos, C. Sander, M. Scharf, The double cube lattice method: efficient approaches to numerical integration of surface area and volume and to dot surface contouring of molecular assemblies, J. Comp. Chem. 16 (1995) 273–284.
[27] D. Eisenberg, A.D. McLachlan, Solvation energy in protein folding and binding, Nature 319 (1986) 199–203.
[28] D. Roccatano, I. Daidone, M.A. Ceruso, C. Bossa, A. Di Nola, Selective excitations of natural fluctuations during thermal unfolding simulations: horse heart cytochrome *c* as a case study, Biophys. J. 84 (2003) 1876–1883.
[29] J. Trewhella, V.A.P. Carlson, E.H. Curtis, D.B. Heidorn, Differences in the solution structures of oxidized and reduced cytochrome *c* measured by small- angle X-ray scattering, Biochemistry 27 (1988) 1121–1125.
[30] A.M. Berghuis, G.D. Brayer, Oxidation state conformational changes in cytochrome *c*, J. Mol. Biol. 223 (1992) 959–976.
[31] A. Dong, P. Huang, W.S. Caughey, Redox-dependent changes in β-extended chain and turn structures of cytochrome *c* in water solution determined by second derivative amide I infrared spectra, Biochemistry 31 (1992) 182–189.
[32] A.A. Kapralov, I.V. Kurnikov, I.I. Vlasova, N.A. Belikova, V.A. Tyurin, L.A. Basova, Q. Zhao, Y.Y. Tyurina, J. Jiang, H. Bayir, Y.A. Vladimirov, V.E. Kagan, The hierarchy of structural transitions induced in cytochrome *c* by anionic phospholipids determines its activation and selective peroxidation during apoptosis in cells, Biochemistry 46 (2007) 14232–14244.
[33] J. Zheng, S. Ye, T. Lu, T.M. Cotton, G. Chunanov, Circular dichroism and resonance Raman comparative studies of WT cytochrome *c* and F82H mutant, Biospectroscopy 57 (2) (2000) 77–84.
[34] T. Takano, O.B. Kallai, R. Swanson, R.E. Dickerson, The structure of ferrocytochrome *c* at 2.45 A resolution, J. Biol. Chem. 248 (1973) 5234–5255.

[35] E. Margoliash, S.F. Miller, J. Tullose, C.H. Kang, B.A. Feinberg, D.L. Brautigan, M. Morrison, Separate intramolecular pathways for reduction and oxidation of cytochrome *c* in electron transport chain reactions, Proc. Natl. Acad. Sci. U.S.A. 70 (1973) 3245–3249.
[36] G.A. Elöve, A.K. Bhuyan, H. Roder, Kinetic mechanism of cytochrome *c* folding: involvement of the heme and its ligands, Biochemistry 33 (1994) 6925–6935.
[37] T.R. Sosnick, L. Mayne, R. Hiller, S.W. Englander, The barriers in protein folding, Nat. Struct. Biol. 1 (1994) 149–156.